Eur. Phys. J. B (2016) 89: 12
DOI: 10.1140/epjb/e2015-60517-3

THE EUROPEAN PHYSICAL JOURNAL B

Regular Article

Duffing revisited: phase-shift control and internal resonance in self-sustained oscillators*

Sebastián I. Arroyo[1,2] and Damián H. Zanette[1,3,a]

[1] Consejo Nacional de Investigaciones Científicas y Técnicas, 1876 Bernal, Argentina
[2] Universidad Nacional de Quilmes, Roque Sáenz Peña 352, 1876 Bernal, Argentina
[3] Centro Atómico Bariloche and Instituto Balseiro, 8400 San Carlos de Bariloche, Argentina

Received 29 June 2015 / Received in final form 7 September 2015
Published online 20 January 2016 – © EDP Sciences, Società Italiana di Fisica, Springer-Verlag 2016

Abstract. We address two aspects of the dynamics of the forced Duffing oscillator which are relevant to the technology of micromechanical devices and, at the same time, have intrinsic significance to the field of nonlinear oscillating systems. First, we study the stability of periodic motion when the phase shift between the external force and the oscillation is controlled – contrary to the standard case, where the control parameter is the frequency of the force. Phase-shift control is the operational configuration under which self-sustained oscillators – and, in particular, micromechanical oscillators – provide a frequency reference useful for time keeping. We show that, contrary to the standard forced Duffing oscillator, under phase-shift control oscillations are stable over the whole resonance curve, and provide analytical approximate expressions for the time dependence of the oscillation amplitude and frequency during transients. Second, we analyze a model for the internal resonance between the main Duffing oscillation mode and a higher-harmonic mode of a vibrating solid bar clamped at its two ends. We focus on the stabilization of the oscillation frequency when the resonance takes place, and present preliminary experimental results that illustrate the phenomenon. This synchronization process has been proposed to counteract the undesirable frequency-amplitude interdependence in nonlinear time-keeping micromechanical devices.

1 Introduction

Since the 1970s, the Duffing oscillator – first introduced by the German engineer Georg Duffing in 1918 [1] – has been repeatedly invoked as a paradigm for nonlinear behavior in classical mechanical systems [2]. The mere addition of a cubic force to a linear damped oscillator deploys a plethora of complex phenomena, but still preserves the simple mathematical form and low dimensionality that makes the system readily amenable to computational exploration and, to a certain extent, to analytical study. Under the action of an external harmonic force, the Duffing oscillator's response can be bistable, with two possible oscillation amplitudes for each frequency. This property, which is directly related to the well-known Duffing leaning resonance curve [3], has been exploited as an illustration of catastrophe theory [4]. If, moreover, the sign of the linear force is inverted, creating a double-well potential, the dynamics can turn into non-periodic motion, with a strange attractor that became a traditional example of low-dimensional chaos [5,6].

Much more recently, the Duffing oscillator acquired relevance in the realm of microtechnologies [7–9]. It has since long been known that the Duffing equation stands for the leading nonlinear correction to the oscillations of an elastic beam clamped at its two ends [10,11]. Minute vibrating silica beams, in turn, have been proposed as pacemakers for the design of time-keeping devices at the microscale, where traditional quartz crystals are difficult to build and operate [7]. To overcome the effect of thermal and electronic noise, these microscopic silica beams must vibrate at relatively large amplitudes. Therefore, their oscillations take place within the nonlinear regime and – in clamped-clamped configurations [8] – the appropriate mathematical description is thus given by the Duffing equation.

In order to function as a pacemaker, a mechanical system must be able to sustain stationary periodic motion with an autonomously generated frequency. This can be achieved in practice by inserting the oscillator into a feedback electronic circuit [12] which, first, reads the signal generated by the oscillator's displacement from equilibrium. This signal is then conditioned by shifting its phase by a prescribed amount (or, equivalently, by inserting a time delay) and fixing its amplitude. Once conditioned, the signal is transformed into a mechanical force and reinjected to act on the oscillator. The oscillator, in turn, responds to this action as an ordinary resonator, except that the "external" force possesses the frequency generated by

* Supplementary material in the form of one pdf file and one gif file available from the Journal web page at http://dx.doi.org/10.1140/epjb/e2015-60517-3

[a] e-mail: zanette@cab.cnea.gov.ar

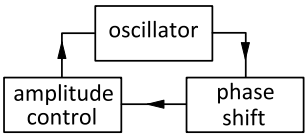

Fig. 1. Schematic representation of the feedback process that stirs self-sustained oscillations. The electric signal produced by the oscillatory motion is conditioned by shifting its phase and adjusting its amplitude, and is then reinjected as a mechanical force acting on the oscillator itself.

the oscillator itself. The result of this feedback process, schematized in Figure 1, is that the mechanical system reaches self-sustained periodic motion, with the only external input of the power needed to condition the electric signal. The frequency of the oscillations is determined by the mechanical properties of the oscillator itself and the parameters of signal conditioning. From the dynamical viewpoint, this self-sustained configuration has the interest that the control parameter, to which the experimenter has access at the conditioning stage, is the phase shift between the oscillation and the force – instead of the frequency, as in the standard case of an externally forced oscillator.

In this paper, we focus on two aspects of the dynamics of the self-sustained Duffing oscillator which, apart from their interest from a theoretical perspective, have specific implications in the technological applications of the system. In both cases, we provide approximate analytical results and a numerical validation. After briefly reviewing the mathematical model and its main properties in Section 2, we first analyze the stability of oscillatory motion under controlling the phase shift between the oscillations and the self-sustaining force (Sect. 3). In contrast with the case where the frequency is controlled, where both stable and unstable solutions are found for a given set of parameters, we find that in our case oscillations are always stable. Additionally, we provide approximate analytical solutions for the transient dynamics of the oscillation amplitude and frequency. Then, in Section 4, we analyze a model for the coupling between the main oscillation mode and a higher-harmonic linear mode in a clamped-clamped oscillator. The ensuing internal resonance, with mutual synchronization of the two modes, has been invoked as a possible method to neutralize the undesirable dependence of the frequency on the amplitude, characteristic of any nonlinear oscillating system [8]. We present an experimental demonstration of the internal resonance under phase-shift control, and fit the experimental results with a simple analytical approximation to the model. Our conclusions are drawn in Section 5.

2 The self-sustained Duffing oscillator

In its main oscillation mode, an elastic beam clamped at its two ends vibrates transversally, much like a plucked string [8]. For moderate amplitudes, the displacement from equilibrium is well-described by a coordinate $x(t)$ satisfying

$$\ddot{x} + Q^{-1}\dot{x} + x + \beta x^3 = f_0 \cos(\phi + \phi_0). \qquad (1)$$

This equation of motion has been normalized by the effective mass, and time units have been chosen in such a way that the frequency of undamped ($Q^{-1} = 0$), harmonic ($\beta = 0$), unforced ($f_0 = 0$) oscillations is equal to one. The quality factor Q gives the ratio between the typical damping time and the oscillation period – or, equivalently, between the width of the resonance curve and the oscillation frequency – and β weights the relative strength of the nonlinear forcing. Clamped-clamped oscillators have $\beta > 0$, so that the nonlinearity hardens the total force.

The right-hand side of equation (1) stands for the self-sustaining force provided by the feedback circuit, as described in the Introduction. Here, $\phi(t)$ is the phase associated to the oscillatory motion, while ϕ_0 and f_0 are the phase shift and the amplitude fixed by signal conditioning (see Sect. 1). For harmonic oscillations, the phase is defined in terms of the coordinate, from the identity $x(t) = A\cos\phi(t)$. For other kinds of motion, the phase can be defined in a variety of ways [13]. Elsewhere, we have discussed analytical and numerical definitions which are especially adapted to our specific problem [14]. In the present contribution, however, we deal mainly with harmonic-like motion.

Assuming that the self-sustained system performs oscillations with constant amplitude and frequency, the simplest approximation to handle the nonlinear effects of the cubic term is to disregard higher-harmonic contributions to the oscillatory motion – as traditionally done for the forced Duffing oscillator [3]. This corresponds to the lower-order approximation in the harmonic balance procedure [15]. We propose a harmonic solution $x(t) = A\cos\phi \equiv A\cos\Omega t$ and neglect higher-harmonic terms by approximating

$$\cos^3\phi = \frac{3}{4}\cos\phi + \frac{1}{4}\cos 3\phi \approx \frac{3}{4}\cos\phi.$$

Separating terms proportional to $\cos\phi$ and $\sin\phi$ yields the algebraic equations

$$(1-\Omega^2)A + \tilde{\beta}A^3 = f_0\cos\phi_0, \quad Q^{-1}\Omega A = f_0\sin\phi_0, \quad (2)$$

with $\tilde{\beta} = \frac{3}{4}\beta$. These equations can be brought to a third-degree polynomial relation between the unknowns, and are therefore explicitly solvable. Figures 2a and 2b show, as solid lines, the solutions for the amplitude A and the frequency Ω as functions of the phase shift ϕ_0, with $Q^{-1} = 0.1$, $\tilde{\beta} = 0.1$, and $f_0 = 1$. In Figure 2c, the graph of amplitude versus frequency yields the typical Duffing resonance curve. Over this curve, $\phi_0 \approx 0$ and π at the leftmost and rightmost ends, respectively. At the peak, where the oscillator's response to the self-sustaining force is maximal, we have $\phi_0 = \pi/2$. For this phase shift, in fact, the force and the velocity $\dot{x}$ oscillate in-phase.

It is important to realize that the functional interdependence between A, Ω, and ϕ_0, given by equations (2), is exactly the same whether the oscillator is subject to the self-sustaining force that fixes the phase shift ϕ_0, or whether it moves under the action of an external force of

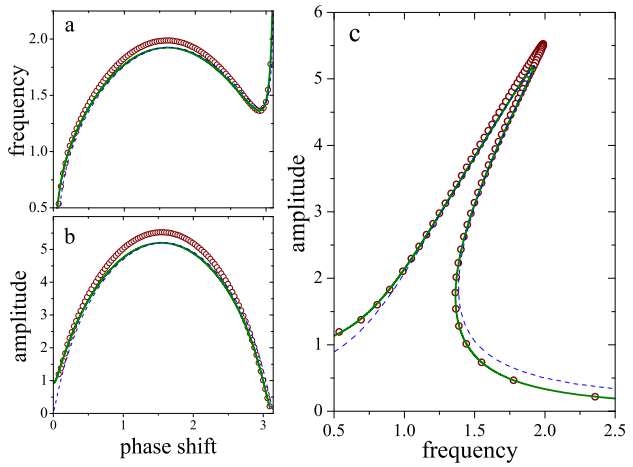

Fig. 2. Interdependence of amplitude, frequency, and phase shift for periodic motion of a forced Duffing oscillator, with $Q^{-1} = 0.1$, $\tilde{\beta} = 0.1$, and $f_0 = 1$. Solid lines: solutions to equations (2); dashed lines: stationary solutions to equations (9); open dots: long-time numerical solutions to the equation of motion of the self-sustained oscillator, equation (1), for numerous values of the phase shift ϕ_0.

given frequency Ω. In particular, the resonance curve in Figure 2c is the same irrespectively of the control parameter being the phase shift or the frequency. In the latter case, it is well known that, within the frequency range where three solutions for the amplitude exist, the two outermost solutions are stable, while the inner solution is unstable [3,16]. On the other hand, the frequency and amplitude plots in Figures 2a and 2b suggest that, as the phase shift is varied, no bifurcations take place, so that stability should not change. In the next section, we show that – in contrast with the standard forced Duffing oscillator – periodic motion under the action of a self-sustaining force with phase-shift control is in fact stable over the *whole* resonance curve.

3 Stability under phase-shift control

Whether the steady oscillations described by equations (2) are stable, and represent the asymptotic motion of the Duffing oscillator, can be decided by a variety of perturbation techniques which, as a byproduct, provide an approximate solution to equation (1) beyond stationary harmonic oscillations. In our case, a convenient approach is provided by the method of multiple time scales [16]. This method discerns between a scale typical of the oscillatory motion, with period of order unity, and a longer time scale characteristic of slow changes in amplitude and frequency. In its usual formulation, the method requires that all forces acting on the oscillator, apart from the linear elastic interaction, are treated as perturbations. Here, we partly relax this requirement by allowing the cubic force to be of the same order as the linear force. Specifically, we rewrite equation (1) as:

$$\ddot{x} + x + \beta x^3 = \epsilon \left[-Q^{-1}\dot{x} + f_0 \cos(\phi + \phi_0) \right], \qquad (3)$$

with ϵ the perturbation parameter. In connection with the applications referred to in the Introduction, this approximation is consistent with the fact that clamped-clamped microoscillators usually have a large quality factor ($Q \sim 10^4$ to 10^5; see also Sect. 4), which implies a small damping force [8,9]. The self-sustaining force, which compensates the energy lost by damping, is also small. On the other hand, due to the large oscillation amplitude needed to overcome the effect of noise, the nonlinear and the elastic forces are generally comparable to each other.

The method of multiple scales assumes that the solution to equation (3), $x(t;\epsilon)$, depends on time through two auxiliary variables, $\tau_0 \equiv t$ and $\tau_1 \equiv \epsilon t$, respectively representing the fast and slow scales, and that it can be expanded as:

$$x(t;\epsilon) = x_0(\tau_0, \tau_1) + \epsilon x_1(\tau_0, \tau_1) + \dots$$

Inserting this ansatz, and taking into account that $\frac{d}{dt} = \partial_0 + \epsilon\partial_1$, where ∂_i indicates partial differentiation with respect to τ_i $(i = 0, 1)$, terms of order ϵ^0 yield

$$\partial_0^2 x_0 + x_0 + \beta x_0^3 = 0. \qquad (4)$$

As a solution to this equation, we propose an oscillation with slowly varying amplitude A, frequency Ω_0, and an additional phase α:

$$x_0(\tau_0, \tau_1) = A(\tau_1)\cos[\Omega_0(\tau_1)\tau_0 + \alpha(\tau_1)]. \qquad (5)$$

Note that the actual frequency of this oscillation is *not* Ω_0 but rather the time derivative of the total phase,

$$\Omega \equiv \frac{d}{dt}(\Omega_0\tau_0 + \alpha) = \Omega_0 + \epsilon(\Omega_0'\tau_0 + \alpha'), \qquad (6)$$

where primes denote ordinary differentiation with respect to τ_1. The oscillation frequency thus differs from Ω_0 by a quantity of order ϵ. Approximating the nonlinear term as explained in Section 2, equation (4) requires that $A(\tau_1)$ and $\Omega_0(\tau_1)$ are related as[1]

$$1 - \Omega_0^2 + \tilde{\beta}A^2 = 0 \qquad (7)$$

for each value of the slow time variable τ_1.

To the first order in ϵ, our formulation yields

$$\partial_0^2 x_1 + x_1 + 3\beta x_0^2 x_1 = -2\partial_0\partial_1 x_0 - Q^{-1}\partial_0 x_0 + f_0\cos(\Omega\tau_0 + \alpha + \phi_0). \qquad (8)$$

Within the same approximation used above to deal with the nonlinear forces, the general solution to this equation contains terms which grow indefinitely as time elapses. These secular contributions, which arise from the resonance between the autonomous oscillations of x_1 and the "external" forcing proportional to the derivatives of x_0, disappear if the following conditions are required to hold:

$$2\left(A'\Omega_0 + A\Omega_0'\right) + Q^{-1}A\Omega_0 = f_0\sin\phi_0,$$
$$2A\Omega_0\left(\Omega_0'\tau_0 + \alpha'\right) = -f_0\cos\phi_0. \qquad (9)$$

[1] This functional relation between amplitude and frequency coincides with the *backbone* approximation of the resonance curve, which we exploit in Section 4.2.

The first of these equations is immediately solved for the product $U = A\Omega_0$, as:

$$U(\tau_1) = Qf_0 \sin\phi_0 + [U(0) - Qf_0 \sin\phi_0]\, e^{-\tau_1/2Q}. \quad (10)$$

Both A and Ω_0 can then be found using equation (7):

$$A^2 = \frac{\sqrt{1+4\tilde{\beta}U^2}-1}{2\tilde{\beta}}, \quad \Omega_0^2 = \frac{\sqrt{1+4\tilde{\beta}U^2}+1}{2}. \quad (11)$$

As for the second of equations (9), comparing with equation (6) we note that, except for a factor ϵ, the parenthesis in the left-hand side is nothing but the difference between Ω_0 and the actual oscillation frequency Ω. Calling $\delta\Omega = \Omega - \Omega_0$ and using the result for $U(\tau_1)$, we have

$$\delta\Omega(\tau_1) = -\frac{\epsilon f_0 \cos\phi_0}{2Qf_0 \sin\phi_0 + 2\,[U(0) - Qf_0 \sin\phi_0]\, e^{-\tau_1/2Q}}. \quad (12)$$

The solutions given in equations (10) and (12) readily show that the stationary values

$$U_\infty = Qf_0 \sin\phi_0, \qquad \delta\Omega_\infty = -\frac{\epsilon Q^{-1}}{2}\cot\phi_0, \quad (13)$$

are in fact reached in the long-time limit from any initial condition and for any parameter set, which proves their global stability. The corresponding stationary values for A and Ω coincide with those of equations (2) up to terms of order ϵ. They are plotted in Figure 2 as dashed lines. The coincidence with the solutions to equations (2) is excellent except for small amplitudes, where the assumption that damping and self-sustaining are much weaker than the cubic force is not well-founded anymore.

The validity of the stability analysis based on equations (9) is in principle limited to the perturbative limit, $\epsilon \to 0$. To decide whether the self-sustained Duffing system exhibits stable oscillations for any value of the phase shift beyond that limit, we implemented a numerical integration of the equation of motion (1). While the equation can be solved by standard techniques – in our case, the second-order Runge-Kutta algorithm – the numerical definition of the phase ϕ in the self-sustaining force requires extending the notion of phase to non-oscillatory behavior. In fact, during the numerical computation of $x(t)$ it cannot be assumed that the motion is always a harmonic oscillation. In a previous publication [14], we have given details on a suitable method to assign an instantaneous phase $\phi(t)$ to any form of $x(t)$, by locally fitting a trigonometric function. Dots in Figure 2 show long-time numerical measurements of amplitude and frequency for $Q^{-1} = 0.1$, $\tilde{\beta} = 0.1$, $f_0 = 1$, and numerous values of ϕ_0, ranging from $\phi_0 \approx 0$ to π at intervals of $0.01\,\pi$. As in the perturbative limit, the solutions over the resonance curve are stable for all ϕ_0. Moreover, the numerical results show that the solution to equations (2) (solid line) gives a very satisfactory description of stationary oscillations, except for the immediate vicinity of the peak. This difference can be ascribed to the effect of disregarding higher-harmonic components in the analytical formulation, whose contribution is expected to become more important as the oscillation amplitude grows.

4 Internal resonance in a clamped-clamped oscillator

As any other elastic body, the clamped-clamped beam has essentially an infinite number of oscillation modes. Nonlinear effects can couple these modes with each other, establishing an interaction in the form of mutual resonant excitation between different forms of oscillatory motion. Specifically, cubic nonlinearities make it possible that oscillations in the main mode synchronize with higher-harmonic modes whose frequency is three (or a multiple of three) times the fundamental frequency.

In a recent experiment [8], a silica clamped-clamped self-sustained microoscillator, about 500 μm long, 3 μm width, and 10 μm thick, was shown to perform oscillations which, at very small amplitudes, had a frequency of approximately 66 kHz. As the amplitude of the self-sustaining force was gradually increased by the experimenter, the amplitude of the oscillations increased as well, and – due to the hardening nonlinearity of the system – so did their frequency. When the frequency attained 68 kHz, however, it was observed that both the amplitude and the frequency ceased to grow, and both quantities reached a wide plateau where they remained practically constant. The self-sustaining force had to reach more than twice its amplitude at the beginning of the plateau for the oscillation amplitude and frequency to regain their growth.

The stabilization of the oscillation amplitude and frequency in the experiment was attributed to the resonant coupling between the main oscillation mode, sustained by the feedback circuit, and a higher-harmonic mode. In fact, finite-element numerical simulations of the clamped-clamped beam showed the existence of a torsional oscillation mode with a natural frequency slightly larger than three times the natural frequency of the main mode. As advanced in the Introduction, the technological interest of this phenomenon resides in the fact that an oscillator functioning in the resonant regime would maintain a very stable frequency, insensible to amplitude fluctuations in the self-sustaining force, thus providing a more reliable frequency reference [17]. From a more fundamental perspective, an interesting aspect of this internal resonance is that nonlinearities play a twofold role in its origin. First, they induce the oscillation frequency to vary with the amplitude and, as a consequence, to reach the value where resonance is possible. Second, they are the source of the coupling between the main oscillation mode and higher harmonics.

In the experiment, the internal resonance was brought about by changing the amplitude f_0 of the self-sustained force. The phase shift in the feedback circuit, on the other hand, was kept constant at $\phi_0 \approx \pi/2$, i.e. close to the peak of the resonance curve, where the oscillator response to self-sustaining was maximal. Here, we show that the internal resonance can also be induced by varying the phase

shift with fixed f_0. To this end, we implement a variation of the theoretical model used to explain the above described experimental results [8].

4.1 Theoretical model

In our description, following Sections 2 and 3, the main oscillation mode is represented by a coordinate $x_1(t)$ satisfying the self-sustained Duffing equation (1). For the sake of simplicity, the higher-harmonic mode is represented by a coordinate $x_2(t)$ satisfying a *linear* unforced oscillator equation. The two equations are coupled to each other through linear interactions. Thus, for the main mode we have

$$\ddot{x}_1 + Q_1^{-1}\dot{x}_1 + x_1 + \beta x_1^3 = f_0\cos(\phi+\phi_0) + J_1 x_2, \quad (14)$$

while for the higher harmonic we have

$$\omega_2^{-2}\ddot{x}_2 + \omega_2^{-1}Q_2^{-1}\dot{x}_2 + x_2 = J_2 x_1, \quad (15)$$

where $J_{1,2}$ are the coupling intensities, and ω_2 is the higher-harmonic frequency (measured in units of the fundamental frequency; see Eq. (1)).

In order to focus on the phenomenon of frequency stabilization, we disregard the tripling of the frequency induced by the cubic nonlinearity, and concentrate on the synchronization of the two modes, assuming that their frequencies are similar. In other words, we take $\omega_2 \gtrsim 1$. We thus look for solutions to equations (14) and (15) where the two modes oscillate with the same frequency and their phases are locked to each other: $x_1(t) = A_1\cos\Omega t$, $x_2(t) = A_2\cos(\Omega t+\psi_2)$. Proceeding as with equation (1), we find the following algebraic equations for the amplitudes $A_{1,2}$, the frequency Ω and the phase difference ψ_2 between the higher-harmonic oscillation and the main mode:

$$\begin{aligned}(1-\Omega^2)A_1 + \tilde{\beta}A_1^3 &= f_0\cos\phi_0 + J_1A_2\cos\psi_2,\\ Q_1^{-1}\Omega A_1 &= f_0\sin\phi_0 + J_1A_2\sin\psi_2,\\ (\omega_2^2-\Omega^2)A_2\cos\psi_2 - \omega_2Q_2^{-1}\Omega A_2\sin\psi_2 &= \omega_2^2J_2A_1,\\ (\omega_2^2-\Omega^2)A_2\sin\psi_2 + \omega_2Q_2^{-1}\Omega A_2\cos\psi_2 &= 0. \quad (16)\end{aligned}$$

As in the case of equations (2), these equations are equivalent to third-degree polynomial relations between the unknowns, and thus can be exactly solved.

Curves in the three panels of Figure 3 illustrate the interdependence between the amplitude A_1, the synchronization frequency Ω, and the phase shift ϕ_0, as determined by equations (16), for $\beta = 0.005$, $f_0 = 1$, $\omega_2 = 1.3$, $Q_1^{-1} = 0.03$, $\omega_2^{-1}Q_2^{-1} = 0.003$, $J_1 = 10^{-4}$, and $J_2 = 1$. Comparison with Figure 2 makes it clear that the overall outline of the curves is the same as for the self-sustained Duffing oscillator considered in Section 3. However, a crucial feature shows up for synchronization frequencies around the higher-harmonic frequency ω_2. In the close-ups of Figure 3c, we see that the resonance

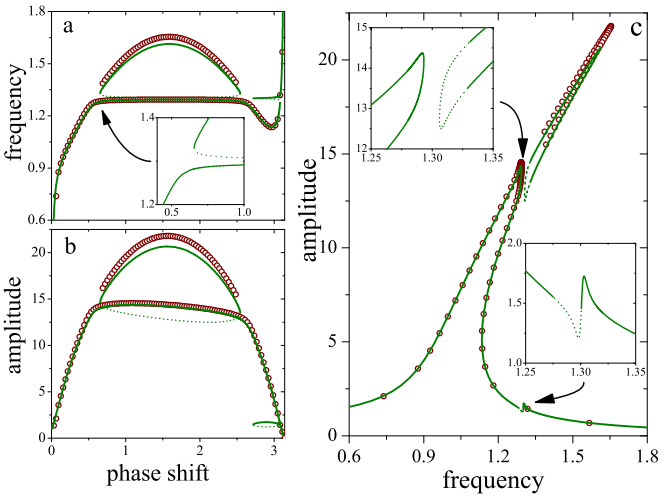

Fig. 3. Interdependence of the amplitude A_1 of the main oscillation mode, the synchronization frequency Ω, and the self-sustaining phase shift ϕ_0, for a forced Duffing oscillator coupled to a linear oscillator representing a higher-harmonic mode. Lines: solutions to equations (16), with $\beta = 0.005$, $f_0 = 1$, $\omega_2 = 1.3$, $Q_1^{-1} = 0.03$, $\omega_2^{-1}Q_2^{-1} = 0.003$, $J_1 = 10^{-4}$, and $J_2 = 1$. Solid and dotted sections represent stable and unstable oscillations, respectively. Open dots: long-time numerical solutions to equations (14) and (15) for the same set of parameters, and numerous values of the phase shift ϕ_0. The insets show close-ups of the zones pointed to by the arrows. For clarity, numerical results are not shown in the insets.

curve develops a gap across the direction of the frequency axis, so that the peak is cut off from the rest of the curve in a kind of elongated "island." For frequencies within the gap, the only possible solution lies on the low-amplitude branch, where the curve acquires in turn an up-down peak whose center and width coincide with those of the gap.

In terms of the variation of the control parameter ϕ_0, in Figure 3a, we see that only one solution exists for small phase shifts, with a rapidly increasing frequency. As ϕ_0 grows further and the frequency approaches that of the higher-harmonic mode, however, the growth of the frequency flattens abruptly and, at the same time, two new solutions appear. Of these two new solutions, the one with the lower frequency remains close to the preexisting solution, with which it determines the frequency gap referred to in the preceding paragraph. Eventually, well beyond the central part of the curves, the two additional solutions disappear and the frequency of the preexisting solution decreases. Note the sizable interval of phase shifts ($0.6 \lesssim \phi_0 \lesssim 2.6$ for the parameters of Fig. 3) along which the preexisting solution maintains its frequency at a practically constant level. For all these values of our control parameter, the main-mode frequency is thus strongly stabilized by the internal resonance. A small additional interval with three solutions, where the frequency is again stabilized, is found for larger values of the phase shift ($2.7 \lesssim \phi_0 \lesssim 3$) in correspondence with the up-down peak of the resonance curve.

From the third and fourth of equations (16) it can be immediately seen that the amplitude of the higher-harmonic mode is:

$$A_2 = \frac{\omega_2^2 J_2 A_1}{\sqrt{(\omega_2^2 - \Omega^2)^2 + \omega_2^2 Q_2^{-2} \Omega^2}}. \quad (17)$$

As expected for a linear oscillator, this amplitude is proportional to the forcing amplitude $J_2 A_1$, but is also modulated by a frequency-dependent Lorentzian factor. This modulation implies that A_2 attains significant values only when the synchronization frequency Ω reaches the vicinity of the higher-harmonic frequency ω_2, i.e. around the frequency gap. Equation (17) also shows that the width of this zone is $\Delta\Omega \sim \omega_2 Q_2^{-1}$, and is therefore inversely proportional to the quality factor of the higher-harmonic mode. It is within this zone that the coupling between the two modes is most effective, and resonant energy transfer takes place from the self-sustained main mode.

Taking into account the results presented in Section 3, the stability of the periodic solutions given by equations (16) can be inferred from a standard analysis of the plot in Figure 3a, which we interpret as a bifurcation diagram for the frequency as a function of the phase shift ϕ_0. Assuming that the solution branches present in both Figures 2 and 3 have the same stability properties, we expect that the only solution found in Figure 3a for small phase shift is stable. The appearance of two new solutions as the phase shift grows should be associated with a saddle-node bifurcation, creating a pair of solutions with opposite stability. The upper branch, also present in Figure 2a, should correspond to the stable one. Upon further increasing of ϕ_0, an inverse saddle-node bifurcation annihilating the same pair takes place and, a little farther, a new saddle-node bifurcation gives rise to the two solutions in the small peak. The unstable solution of this new pair annihilates in turn with the preexisting stable solution, while its stable partner subsists until the phase shift attains its largest values, constituting the rightmost branch of the bifurcation diagram.

We have verified these conclusions on the stability properties of the periodic solutions by numerically solving the equations of motion, with the same scheme as in Section 3. Dots in Figure 3 show long-time numerical measurements of amplitude and frequency with the same parameter choice as for the curves. The control parameter ϕ_0 varies from $\phi_0 \approx 0$ to π at intervals of $0.01\,\pi$. In the zones where three solutions exist, we have integrated the equations of motion at least twice, starting from different initial conditions, compatible with large and small oscillation amplitudes. In the small interval corresponding to the up-down peak, we have refined the phase-shift sampling to get better evidence on the stability of the three solutions. For the sake of clarity, numerical results in this interval are not included in Figure 3.

As Supplementary material*, in order to illustrate how the three main plots of Figure 3 connect with each other, we provide an animation with rotating views of the resonance curve in the three-dimensional space spanned by the coordinates (ϕ_0, Ω, A_1). The resonance curve for a forced *linear* oscillator with the same Q and f_0 is plotted for comparison.

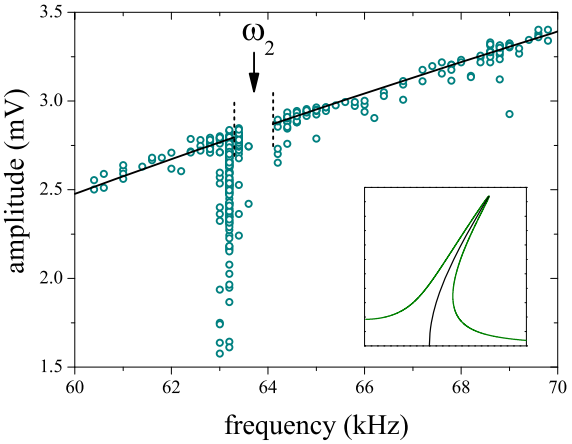

Fig. 4. Experimental measurements (dots) of the amplitude A_1 and frequency Ω of the main oscillation mode under phase-shift control of a self-sustained clamped-clamped microoscillator. Experimental errors (not displayed) were estimated in 0.015 mV for the amplitude and 0.1 kHz for the frequency. Vertical dashed segments indicate the frequency gap caused by the internal resonance, around $\omega_2 \approx 63.7$ kHz. The solid line is a fit of the experimental data with the backbone approximation to our analytical model. The inset illustrates the backbone approximation for a resonance curve with the parameters of Figure 2 ($Q = 10$). The approximation improves sharply as Q grows.

4.2 Preliminary experimental results and the backbone approximation

As mentioned above, previous experiments on frequency stabilization by internal resonance in clamped-clamped microoscillators were carried out for fixed phase shift ($\phi_0 \approx \pi/2$) and varying the amplitude of the self-sustaining force [8]. Under these conditions, due to the effect of the cubic force, the oscillation frequency increases with the amplitude until it reaches the resonance region. The results of Section 4.1, in turn, show that the resonance can also be induced by keeping the self-sustaining amplitude fixed and varying the phase shift.

We have performed preliminary measurements under phase-shift control on the same kind of self-sustained microoscillators as used in previous experiments. In our experiment, the phase shift is tuned by means of a variable resistor in an all-pass filter. As Supplementary material*, we provide diagrams of the circuits used for phase shift and amplitude control. Dots in the main plot of Figure 4 stand for our measurements in the amplitude-frequency plane, i.e. over the resonance curve. The amplitude is measured from an oscillating electric signal produced by the vibrating silica bar through a capacitive transducer, and is therefore given in millivolts. The uncertainty in the determination of amplitude and frequency is around 0.015 mV and 0.1 kHz, respectively.

As the phase shift is increased from small values, first, the frequency and the amplitude grow as well. Then, when the frequency reaches some 63.3 kHz, the oscillations suddenly become irregular, with their amplitude varying erratically over a considerably wide interval. The frequency, on the other hand, remains stable at a rather well-defined value, insensible to the amplitude fluctuations. Frequency stabilization is apparent at this point. Further increase of the phase shift leads again to more stable oscillations, regaining the regime where both the amplitude and the frequency grow with ϕ_0. A gap, however, has been left vacant for frequencies between 63.3 and 64.1 kHz, corresponding to amplitudes between 2.8 and 2.9 mV, approximately.

Our experimental results can be satisfactorily fitted by the model presented in Section 4.1, with a suitable choice of its parameters. To this end, it is useful to note first that the quality factor of a clamped-clamped silica microoscillator as used in the experiments is typically in the order of 10^4 to 10^5 [8]. This large quality factor implies that the Duffing resonance curve is very narrow, with its two leaning branches very close to each other. Under these conditions, the two branches are well represented by a single curve – sometimes called *backbone* curve [16] – given by an approximate expression for the interdependence between amplitude and frequency. The inset of Figure 4 shows a resonance curve with $Q = 10$ and its backbone approximation. As Q grows and the curve becomes narrower, the approximation is increasingly good.

The backbone approximation for the Duffing resonance curve is obtained from equations (2) by neglecting the contribution of damping and of the external force. With the notation of equations (2), the backbone curve is given by:

$$A = \sqrt{(\Omega^2 - 1)/\tilde{\beta}}.$$

The value of the phase shift ϕ_0 along the curve can then be determined from the second of those equations: $\sin\phi_0 = \Omega A/Qf_0$. In order to fit the experimental data outside the internal-resonance gap, and taking into account the above functional relation between amplitude and frequency along the backbone curve, we propose the fitting function

$$A_1 = a_1\sqrt{(\Omega/\omega_1)^2 - 1}, \tag{18}$$

where the tunable parameters a_1 and ω_1 account for the units of measure of A_1 and Ω in the experiment. Our estimate yields $a_1 = (6.4 \pm 0.1) \times 10^{-2}$ mV, and $\omega_1 = (46 \pm 1)$ kHz. The line in the main plot of the figure stands for this estimate. Assuming for our microoscillator a quality factor of the order of 10^4 or larger, the width of the resonance curve would fall well inside the dispersion of the experimental data, which justifies using the backbone approximation.

To fit the gap in the backbone curve, indicated by vertical dashed lines in Figure 4, we now turn the attention to equations (16). Solving the two last equations for the product $A_2\sin\psi_2$, and replacing the result into the second equation, makes it possible to write

$$\sin\phi_0 = \left[1 + \frac{\nu^4}{(\omega_2^2 - \Omega^2)^2 + \omega_2^2 Q_2^{-2}\Omega^2}\right]\sin\Phi_0. \tag{19}$$

The constant ν^4 – where ν has units of frequency – is proportional to the product of the coupling constants, J_1J_2, and to the ratio of the quality factors of the two involved oscillation modes, Q_1/Q_2. These quantities cannot be discerned from each other in our experiment, and ν must therefore be considered as a single fitting parameter. The angle Φ_0, in turn, can be associated to the phase shift in the zone of the gap when the internal resonance is absent, i.e. for $\nu^4 \propto J_1J_2 = 0$. From our measurements of amplitude and frequency as functions of the phase shift (not presented here) we estimate $\sin\Phi_0 = 0.16 \pm 0.01$.

Equation (19) makes it clear that the gap in the backbone curve appears when the second term inside the square bracket in the right-hand side is large enough as to make $\sin\phi_0 > 1$, for which no real value of the phase shift ϕ_0 satisfies the equation. The Lorentzian profile of this term as a function of the frequency Ω indicates that the gap occurs around ω_2. As advanced in Section 4.1, its width $\Delta\Omega$ is proportional to $\omega_2 Q_2^{-1}$. Locating the center of the gap, we estimate $\omega_2 = (63.7 \pm 0.2)$ kHz. Tuning the constant ν, on the other hand, requires knowing the quality factor Q_2 of the higher-harmonic mode, to which we do not have access in the experiment. However, if – in the spirit of the backbone approximation – we assume that Q_2 is large, the contribution of the term $\omega_2^2 Q_2^{-2}\Omega^2$ in the denominator of the Lorentzian function can be neglected by comparison to $(\omega_2^2 - \Omega^2)^2$. Within this assumption, we find $\nu^4 = (\omega_2\Delta\Omega)^2(1 - \sin\Phi_0)/\sin\Phi_0$. Taking $\Delta\Omega = 0.8$ kHz, our estimate yields $\nu = (10.8 \pm 0.2)$ kHz.

5 Conclusion

Micromechanical devices have opened the possibility of renewed mutual contribution between nonlinear physics and technological applications [7,18]. On one side, this minute machines – still belonging to the realm of Newtonian mechanics – often function within regimes where nonlinear effects play a substantial role in the dynamics. This is particularly true for micromechanical oscillators, which are foreseen to be used as pacemakers in time-keeping electronic devices, and whose large vibration amplitudes bring them well beyond the linear elastic regime. On the other side, well-developed techniques of MEMS fabrication can be used to build up microscale lab equipment, where complex physical phenomena such as the collective dynamics of large populations of nonlinear coupled oscillators may be realized and tested. This path is just beginning to be explored [19,20].

In this paper, we have studied two technologically relevant aspects of the self-sustained Duffing oscillator, which models a clamped-clamped elastic bars inserted in a feedback circuit. Firstly, following a variant of the traditional multiple-scale approach used to study the stability of the standard Duffing equation [16], we have shown

that the self-sustained oscillator is stable along the entire resonance curve. This result, already advanced in reference [12], has here been obtained without assuming that the nonlinear force is a perturbation to the linear interaction, which is consistent with realistic conditions in the operation of micromechanical oscillators. Stability along the whole resonance curve contrasts with the well-known standard behavior, where an unstable branch develops in the middle part of the curve. The difference resides in the fact that, in the self-sustained oscillator, the system is controlled by fixing the phase shift between oscillation and forcing whereas, in the standard case, the control parameter is the forcing frequency. The situation is reminiscent – although not fully equivalent – to the basic process of feedback stabilization prescribed by control theory [21]. We have shown that, within the multiple-scale approximation, the equations of motion can be exactly solved, and provided numerical evidence that validate the approximation.

In the second place, we have elaborated on a model for the internal resonance between the main oscillation mode and a higher-harmonic mode in a clamped-clamped oscillator. The interest of this phenomenon lies in that it has been associated with the frequency stabilization observed in microoscillators upon variation of the forcing amplitude [8]. Frequency stability under amplitude fluctuations is an unavoidable condition for the use of microoscillators as frequency references in time-keeping devices. The model describes the internal resonance as a synchronization process between the main nonlinear oscillation, represented by the self-sustained Duffing equation, and a linear oscillator of different frequency coupled to the main mode. Due to this phenomenon, the Duffing resonance curve develops a gap, which is associated to a wide phase-shift interval where the oscillation frequency remains practically constant. A similar "island" effect has recently been reported for an externally forced Duffing oscillator coupled through displacement and velocity to a linear oscillator [22]. It is interesting to point out that, in the vicinity of the gap, the amplitude-frequency interdependence is similar to that of the standard forced Duffing oscillator at its subharmonic resonances [16]. In order to establish the stability properties of the model, we have performed numerical simulations. These support a picture where the resonance occurs through two pairs of direct-inverse saddle-node bifurcations. Finally, we have presented preliminary experimental results which illustrate the internal resonance in the situation where, contrary to previous experiments, the phase shift between forcing and oscillation was controlled. Model and experiment were fitted to each other within a high-quality-factor approximation.

At the microscale, an important dynamical ingredient – that has however been purposely left aside in our description – is added by noise. Random fluctuations of both thermal and electronic origin become increasingly influential on the mechanics of micromachines as these decrease in size. In the case of oscillators, noise makes it necessary to work at larger amplitudes, which in turn increases the effects of nonlinearities. To our knowledge, a theoretical approach to the interplay between noise and nonlinearities focused on the dynamics of micromechanical systems is still lacking. This seems to be an appealing next step in the lines of the present research, where the physics of stochastic processes should have their say.

Author contribution statement

S.I.A. and D.H.Z. contributed equally to the paper.

We acknowledge financial support from ANPCyT (PICT 2011-0545 and 2014-1611), Argentina, and enlightening discussions with Hernán Pastoriza, Darío Antonio, and Daniel López. Experiments were conducted at the MEMS Laboratory of Centro Atómico Bariloche.

References

1. G. Duffing, *Erzwungene Schwingungen bei Veränderlicher Eigenfrequenz* (F. Vieweg u. Sohn, Braunschweig, 1918)
2. I. Kovacic, M.J. Brennan, *The Duffing Equation: Nonlinear Oscillators and Their Behaviour* (Wiley, New York, 2011)
3. L.D. Landau, E.M. Lifshitz, in *Mechanics. Course of Theoretical Physics* (Butterworth-Heinemann, Oxford, 1976), Vol. 1
4. P.J. Holmes, D.A. Rand, J. Sound Vibr. **44**, 237 (1976)
5. P.J. Holmes, Phil. Trans. R. Soc. A **292**, 419 (1979)
6. P.J. Holmes, D. Whitley, Physica D **7**, 111 (1983)
7. K.L. Ekinci, M.L. Roukes, Rev. Sci. Instrum. **76**, 061101 (2005)
8. D. Antonio, D.H. Zanette, D. López, Nat. Commun. **3**, 806 (2012)
9. D.K. Agrawal, J. Woodhouse, A.A. Seshia, IEEE Trans. Ultrason. Ferroelectr. Freq. Control **60**, 1646 (2013)
10. R. Narashima, J. Sound Vib. **8**, 134 (1968)
11. T.C. Molteno, N.B. Tufillaro, Am. J. Phys. **72**, 1157 (2004)
12. B. Yurke, D.S. Greywall, A.N. Pargellis, P.A. Busch, Phys. Rev. A **51**, 4211 (1995)
13. Y. Kuramoto, *Chemical Oscillations, Waves, and Turbulence* (Springer, Berlin, 1984)
14. S.I. Arroyo, D.H. Zanette, Phys. Rev. E **87**, 052910 (2013)
15. T. Detroux, L. Renson, G. Kerschen, in *Nonlinear Dynamics, Conference Proceedings of the Society for Experimental Mechanics Series*, edited by G. Kerschen (Springer, Berlin, 2014), Vol. 2, Chap. 3
16. A.H. Nayfeh, D.T. Mook, *Nonlinear Oscillations* (Wiley, New York, 1995)
17. M. Agarwal, S.A. Chandorkar, H. Mehta, R.N. Candler, B. Ki, M.A. Hopcroft, Appl. Phys. Lett. **92**, 104106 (2008)
18. L.G. Villanueva, R.B. Karabalin, M.H. Matheny, D. Chi, J.E. Sader, M.L. Roukes, Phys. Rev. B **87**, 024304 (2013)
19. D.K. Agrawal, J. Woodhouse, A.A. Seshia, Phys. Rev. Lett. **111**, 084101 (2013)
20. M.H. Matheny, M. Grau, L.G. Villanueva, R.B. Karabalin, M.C. Cross, M.L. Roukes, Phys. Rev. Lett. **112**, 014101 (2014)
21. E.D. Sontag, in *Robust Control of Linear Systems and Nonlinear Control. Progress in Systems and Control Theory*, edited by M.A. Kaashoek, J.H. van Schuppen, A.C.M. Ran (Birkäuser, Boston, 1990), Vol. 4, p. 61
22. G. Habib, T. Detroux, R. Viguié, G. Kerschen, Mech. Sys. Sig. Proc. **52-53**, 17 (2015)